Chinese Chemical Letters 32 (2021) 3202–3206

Contents lists available at ScienceDirect

Chinese Chemical Letters

journal homepage: www.elsevier.com/locate/cclet

Communication

Capture and separation of CO_2 on BC_3 nanosheets: A DFT study

Houyong Yang[a,b], Chaozheng He[a,b,*], Ling Fu[c,**], Jinrong Huo[d], Chenxu Zhao[a,b], Xiuyuan Li[a,b], Yan Song[a,b]

[a] Shaanxi Key Laboratory of Optoelectronic Functional Materials and Devices, School of Materials Science and Chemical Engineering, Xi'an Technological University, Xi'an 710021, China
[b] Institute of Environmental and Energy Catalysis, School of Materials Science and Chemical Engineering, Xi'an Technological University, Xi'an 710021, China
[c] College of Resources and Environmental Engineering, Tianshui Normal University, Tianshui 741001, China
[d] School of Sciences, Xi'an Technological University, Xi'an 710021, China

ARTICLE INFO

Article history:
Received 2 December 2020
Received in revised form 18 December 2020
Accepted 25 January 2021
Available online 30 March 2021

Keywords:
Hexagonal
BC_3
Electric field
Density functional theory
CO_2 capture and separation

ABSTRACT

In order to reduce the greenhouse effect caused by the rapid increase of CO_2 concentration in the atmosphere, it is necessary to develop more efficient, controllable, and highly sensitive adsorbing materials. In this study, the adsorption behavior of CO_2 on BC_3 nanosheets under an external electric field was explored based on density functional theory (DFT). It was found that CO_2 experienced a transition from physisorption to chemisorption in the electric field range of 0.0060-0.0065 a.u.. In addition, the adsorption/desorption of CO_2 is reversible and can be precisely controlled by switching on/off at the electric field of 0.0065 a.u.. The selective adsorption of $CO_2/H_2/CH_4$ by BC_3 can also be used to realize gas separation and purification under different electric fields. This study highlighted the potential application of BC_3 nanosheets as a high-performance, controllable material for CO_2 capture, regeneration, and separation in an electric field.

CO_2 capture and storage has attracted extensive research due to the greenhouse effect caused by its concentration rapid increase, which caused environmental deterioration and global warming. It is necessary to consider the nature of the adsorbent materials containing the high adsorption capacity, sensitive selectivity [1], low energy consumption during adsorption/desorption process, more reusable times [2,3] and structural stability [4]. At present, the popular CO_2 adsorbents are the metal-organic frameworks (MOFS) [5,6], covalent organic frameworks (COFS) [7], 2D solid materials including graphene [8], graphene-like materials [9], porous carbon materials and polymers [10–13].

In the past few years, many researches have been done on the use of external electric fields to promote CO_2 adsorption and achieve CO_2 separation. Guo *et al*. found that the hexagonal BN nanosheets have high-efficiency adsorption and large capacity for CO_2 under an applied electric field, which is effectively separate CO_2 from the $CO_2/H_2/N_2/CH_4/CO/H_2O$ mixture [14]. The work of Adnan *et al*. shows that under an external electric field of 0.013 a.u., CO_2 achieves the transition from physisorption to chemisorption, while the desorption of CO_2 is a spontaneous exothermic process with 0.06 eV after the removal of electric field [13]. Qiao *et al*. reports that CO_2 capture/regeneration on MoS_2 monolayers can be controlled by external electric fields, and the adsorbed CO_2 can be released without any energy barrier once the electric field is turned off [15].

Recently, BC_3 monolayer with high crystalline quality has been successfully created by carbon-substituted technique in a boron hexagonal comb [16]. BC_3 has excellent mechanical properties [17,18] and thermal stability [19]. It has excellent performance in catalytic reactions [20], and the potential application for gas sensors [21,22].

The first principle is the ab initio calculation, which does not need any parameters. It only needs to start from the most basic physical principle to directly solve the Schrodinger equation with some approximated algorithm, according to the interactions between nucleus and electron and its basic motion rules. The first principle is widely used to calculate the catalysis process of single atom supported or bimetallic catalysts [23–25], chemical reactions caused by external electrical fields [26,27], surface adsorption and activity [28], organics degradation simulation [29], analysis of photocatalytic mechanism [30,31], optical properties prediction [32] and so on [33–45].

* Corresponding author at: Shaanxi Key Laboratory of Optoelectronic Functional Materials and Devices, School of Materials Science and Chemical Engineering, Xi'an Technological University, Xi'an 710021, China
** Corresponding author.
E-mail addresses: hecz2019@xatu.edu.cn (C. He), ful263@nenu.edu.cn (L. Fu).

https://doi.org/10.1016/j.cclet.2021.03.038

In this research, we systematically explored whether BC_3 has the potential to control capture and release of CO_2 under an external electric field. First, the adsorption of $CO_2/H_2/CH_4$ on BC_3 surface was studied, then the transformation of CO_2 adsorption behavior under gradient electric field and the thermodynamic process of CO_2 adsorption/desorption on the surface of BC_3 were further explored. Finally, the application of different electric field values to separate $CO_2/CH_4/H_2$ mixed gas was evaluated.

All of the spin-polarized DFT calculations were performed using the Dmol^3 [46] software. Generalized gradient approximation (GGA) formulated by Perdew, Burke, and Ernzerhof (PBE) are carried out to describe the exchange-correlation energy functional [47], and meanwhile we used all-electron core treatment for the electron ion-core interactions [48], and a double numerical basis set containing d polarization function, such as double numeric with polarization (DNP) to increase accuracy. The spin polarization is turned on all the way, and Grimme method was applied to describe the van der Waals interactions [49]. The charge distributions and the charge transfer between BC_3 monolayer and molecules were analyzed by using Hirshfeld method. For geometry optimization and electronic self-consistency, the convergence tolerance is set to 1×10^{-6} a.u. The convergence threshold parameters of geometric optimization are specified as 1×10^{-5} Ha, 2×10^{-3} Ha/Å and 5×10^{-3} Å for energy, maximum force and displacement, respectively. In the process of structural optimization, the coordinates of the internal atoms were relaxed with the fixed lattice parameters.

The Brillouin k-point grid was sampled by the $6 \times 6 \times 1$ Monkhorst packt grid [50]. The BC_3 base model used 2×2 supercell cotaining 32 atoms with a 20 Å vacuum layer to weaken interaction between layers. The optimized lattice constant of the BC_3 structure is 10.35 Å, which is well consistent with the theoretica1 result of 10.33 Å [51]. Then the adsorption energy was calculated by this formula (Eq. 1):

$$E_{ads} = E_{All} - E_{sub} - E_{gas} \quad (1)$$

Where E_{All} is the total energy of the absorbed combination, E_{sub} and E_{gas} represent the energy of separate BC_3 substrate and gas molecules, respectively. It is worth noting that the E-field perpendiculars to the BC_3 surface and points downward.

As shown in Fig. S1a (Supporting information), BC_3 nanosheets has a planar hexagonal honeycomb structure, each structural unit includes four C atoms and two B atoms. Each B atom was combined with three C atoms *via* sp^2 hybridization. The lengths of B—C and C—C are 1.565 and 1.422 Å, respectively, which was well consistent with the early literature [52]. As depicted in the Fig. S1a, six adsorption sites are considered for molecular adsorption, including the top sites of B (T1) and C (T2) atoms, the bridge sites of C—C (B1) and B—C bond (B2), and the central position of C_4B_2 six-membered ring (H1) and the C six-membered ring (H2).

The structural stability of BC_3 nanosheets under the application of an E-field can be roughly evaluated by the polymerization energy and molecular dynamics simulation. The formula for polymerization energy was defined as Eq. 2:

$$E_{coh} = (nE_B + mE_C - E_{BC_3})/(m+n) \quad (2)$$

Where E_B, E_C, E_{BC_3} represents the energy of B and C atoms and BC_3 nanosheets, respectively, n and m are the number of C and B atoms [53]. As shown in Fig. S1b (Supporting information), as the E-field strength increased from 0 to 0.008 a.u., the average binding energy decreased from 7.52 eV to 7.40 eV. Compared with that of no E-field, the average binding energy between BC_3 atoms changes little, indicating that the structure is stable. For the optimized structure under the electric field the microcanonical ensemble(NVE) ensemble was adopted, at 300 K, molecular dynamics simulation was done. As shown in Fig. S1c (Supporting information), the energy change of the structure is very small in the 2 ps interval of 1 fs, which also confirmed the stability of the BC_3 structure under the applied E-field.

We studied three molecules (CO_2, CH_4, H_2) adsorption on BC_3 substrate, the most stable adsorption structure and relative adsorption parameters were depicted in Fig. S2 and Table S1 (Supporting information), respectively. As shown in Fig. S2, CO_2 tends to adsorb on H1 site of C_4B_2 six-membered ring, however, CH_4 and H_2 tend to adsorb on T2 and T1 sites, respectively. No chemical bond is formed between the molecules and the substrate, where the CO_2, CH_4, H_2 are suspended above the surface. The minimum distance (D_m) between molecules and BC_3 substrate are 3.271, 3.609 and 3.158 Å for CH_4, CO_2 and H_2, respectively, and the corresponding adsorption energy is very small with the value of −0.11, −0.09 and −0.07 eV, respectively. From the analysis of Hirshfeld-type charge transfer, the amount of charge transfer between gas molecules and BC_3 is also very small (0.004 e, −0.025 e and 0.012 e).

As we all know, the strong interactions of the adsorbates combined with surface contribute to the evident results of gas detection selectivity [54] and sensitivity. In order to enhance the CO_2 sensitivity, we apply a forward E-field perpendicular to the Z axis [55] on BC_3 surface [52]. The corresponding adsorption configurations were presented in Fig. 1. According to the difference charge density, the adsorption effect gradually increases along with the increasing of the electric field strength. As shown in Fig. 1c, the angle of ∠O-C-O decreased sharply from 180° to 158.6° along with the electric field increased from 0 to 0.006 a.u., and the adsorption distance reduced from 3.10 Å to 2.94 Å. The adsorption energy adds up to –0.43 eV, and the charge transfer amount increases to 0.2 e, the charge density expands a lot resulting a stronger chemical adsorption. When the electric field value further increased to 0.008 a.u., the distance between CO_2 an-d BC_3 suddenly decreased to 1.75 Å, the angle of ∠O-C-O further decreased to 127.3°, and the amount of charge transfer increased to 0.9 e. Seen from the Fig. 1d, the charge density between CO_2 and BC_3 increased dramatically, resulting that the interaction between the CO_2 molecular and the BC_3 surface has been greatly improved. These evidences indicate that under an applied electric field of 0.008 a.u., CO_2 is chemically adsorbed on the surface of BC_3. It is

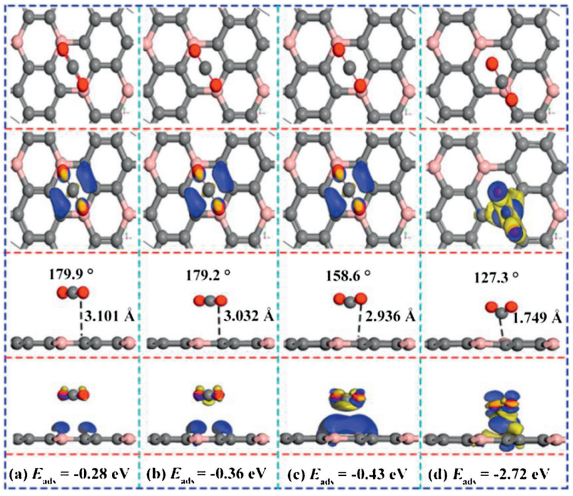

Fig. 1. Top and side views of the most favorable CO_2 adsorption configurations, corresponding charge density difference in an external E-field of (a) 0.002 a.u., (b) 0.004 a.u., (c) 0.006 a.u., (d) 0.008 a.u.. The blue (yellow) color represents accumulation (diminishing) of electrons. The values of isosurface of (a-c) are 0.003 e/Å^3, and (d) is 0.02 e/Å^3.

clearly that CO_2 is 'fixed' to BC_3 surface *via* employing an electric field. The results indicate the interaction between CO_2 and BC_3 surface is enhanced, which cause the stronger gas monitoring sensitivity.

In order to explain the turning point of CO_2 adsorption affected by the electric field, three values of electric field (0.0065, 0007, 0.0075 a.u.) were performed to explore the corresponding adsorption structure, adsorption energy and the differential charge density (as shown in Fig. 2). As shown in Fig. S3a (Supporting information), the adsorption distance suddenly decreased from 1.97 Å under the electric field value of 0.0065 a.u., which was 33% shorter than that of values at 0.006 a.u. (2.94 Å). It is noted that the adsorption energy was increased to –0.84 eV, which is almost diploid compared with that of –0.43 eV. In addition, the angle of ∠O-C-O is reduced to 137.5°, due to the strong interaction of electrons accumulate between CO_2 and the substrate, which indicates that can be regarded as strong chemisorption. When the E-field value increased to 0.0075 a.u., the adsorption distance was further shortened to 1.772 Å, the angle of ∠O-C-O was further reduced to 128.2°, and the adsorption energy was increased to –2.25 eV, which indicates that the interaction between CO_2 and BC_3 substrate is further enhanced. The applied E-field will promote the polarization of the charged particles [56,57], which will lead to the enhanced adsorption of CO_2 on the surface of BC_3 [55]. As shown in Figs. S3a–c (Supporting information), the critical point of CO_2 from physical adsorption to chemical adsorption on the BC_3 substrate is between 0.006-0.0065 a.u.. As shown in Fig. S4, the minimum E-field value (0.0065 a.u.) required for the conversion of CO_2 from physical adsorption to chemical adsorption is much smaller than that of Penta-graphene [4], and is also smaller than the E-field value required in the previous literature to capture CO_2 materials, such as C_2N [55], h-BN [27], C_3N [58], P-doped C_{60} [59], P-doped graphene [60]. It is a pity that the value is just slightly larger than that of MoS_2 [29] and PC_5 [24]. Such as it is, BC_3 captures CO_2 is more economical and efficient.

In order to further study the interaction between CO_2 and BC_3 substrate under different E-field values, partial density of states (PDOS) was studied and presented in Fig. S5 (Supporting information). As shown in Fig. S5, between the E-field value of 0 ∼ 0.004 a.u., there is almost no overlap [48] between the orbits of CO_2 and B atoms, which indicates that the interaction between them is relatively weak physical adsorption. At this time, the E-field has little effect on the capture of CO_2. However, when the E-field value increases to 0.006 a.u., it can be seen that the overall PDOS has a significant right shift, and there is a clear overlapped orbitals of 2p (CO_2) and 2p (B) between 3.0 ∼ 5.0 eV, indicating the adsorption effect was enhanced, similarly as the previous results [52]. Similarly, when the E-field values at 0.0065 and 0.007 a.u., the orbital overlap formed by the 2p (CO_2) and 2p (B) hybrid contributions can appear at –5.5, –1.2 and 5.0 eV, and the same results can be seen at 0.0075 and 0.008 a.u. It should be noted that the applied E-field can significantly enhance the ability of BC_3 to capture CO_2.

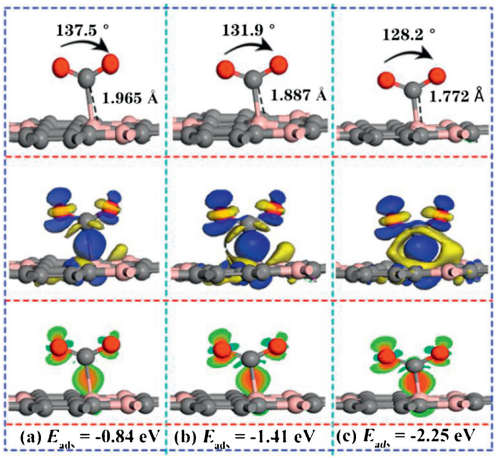

Fig. 2. The side view of the most stable configurations and corresponding charge density difference in E-field of (a) 0.0065 a.u., (b) 0.007 a.u., (c) 0.0075 a.u.. The blue (yellow) color represents accumulation (diminishing) of electrons. Red and green represent increasing and decreasing electron density. The values of isosurface of (a), (b), (c) are 0.015 e/Å^3, respectively.

In order to further study the mechanism of CO_2 adsorption on BC_3 under an external E-field, the crystal orbital hamiltonian population (COHP) was performed to analyze the different adsorption structures [61–64]. As shown in Fig. 3, the red area is the contribution of the anti-bonding state, and the cyan area is the bonding state. Fig. 3a shows that in the absence of an external E-field, the molecular orbital between C–O is composed by the $\sigma_{s\text{-}p}$ bonding orbital (at –6.8 eV) that formed by the interaction of C_s and O_p and the anti-bonding $\pi^*_{p\text{-}p}$ (at 4.5 eV) formed by the interaction of C_s and O_p. In addition, integrated COHP (ICOHP) was calculated to analyze the energy integral up to the highest occupied bands, and the value of ICOHP quantitatively reflected the strength of bonding. As shown in Figs. 3a–d, as the value of the E-field increases, ICOHP gradually decreases, which indicating the weaker of C—O bond in CO_2. The reason is that with the increases of the E-field, the interaction between the C of CO_2 and B atom is enhanced, inducing the electron cloud more shared with the B atom and a reduction in the overlap of the electron cloud of the C-O, which is accordance with the weakened C—O interaction. Figs. S6a–d show that as the E-field strength increases, the ICOHP between C and B atom increases with the bonding state broaden, indicating that the interaction between C and B is strengthen. It should be highlighted that in the range of 0.0065-0.0075 a.u., the bonding molecular orbital $\sigma_{p\text{-}p}$ between C and B atoms is mainly composed by C_p and B_p. Interestingly, bonding molecular orbitals $\sigma_{p\text{-}p}$ which located in lower energy contributed by C_p and B_p appeared near the Fermi level.

In order to further explore the possible mechanism of CO_2 adsorption and desorption on BC_3 substrate under the external E-field existence, the potential energy [65] surface was shown in Fig. 4. The energy of the CO_2 adsorption system without an E-field is defined as 0. Clearly, the energy of the system gradually decreases along with E-field increases, indicating that the adsorption of CO_2 under the external E-field is a spontaneous exothermic process. In addition, when applying 0.006 a.u. E-field, the relative system energy decreases to –0.26 eV. It is worth noting that when the external E-field increases to 0.0065 a.u., the relative energy difference immediately decreases to –0.69 eV, well consistent with the E_{ads} of –0.84 eV, resulting to strong chemical adsorption. Besides, we also systematically studied the capture and separation of CO_2 gas on the BC_3 substrate by switching the E-field. As shown in Fig. 4b, under the external electric field of 0.0065 a.u., CO_2 is chemically adsorbed on the surface of BC_3. When the external electric field is turned off, the CO_2 adsorption distance is extended from 1.965 Å to 3.264 Å with the CO_2 angle shifted from 137.5° to 179.9° after restructuring optimization. The above results demonstrate that the removal of the electric field can promote the transition from chemical adsorption to physical adsorption, in this process the endothermic reaction relative energy value is 0.69 eV. Similarly, when the E-field is switched on, CO_2 changed from physical adsorption to chemical adsorption with a linear structure to a V-shaped structure, and the adsorption distance is shortened to 1.965 Å. This process is exothermic process with relative energy –4.06 eV without energy barrier. These results shows that the adsorption/desorption of CO_2 on the BC_3 substrate can be easily controlled by the opening/closing of the electric field.

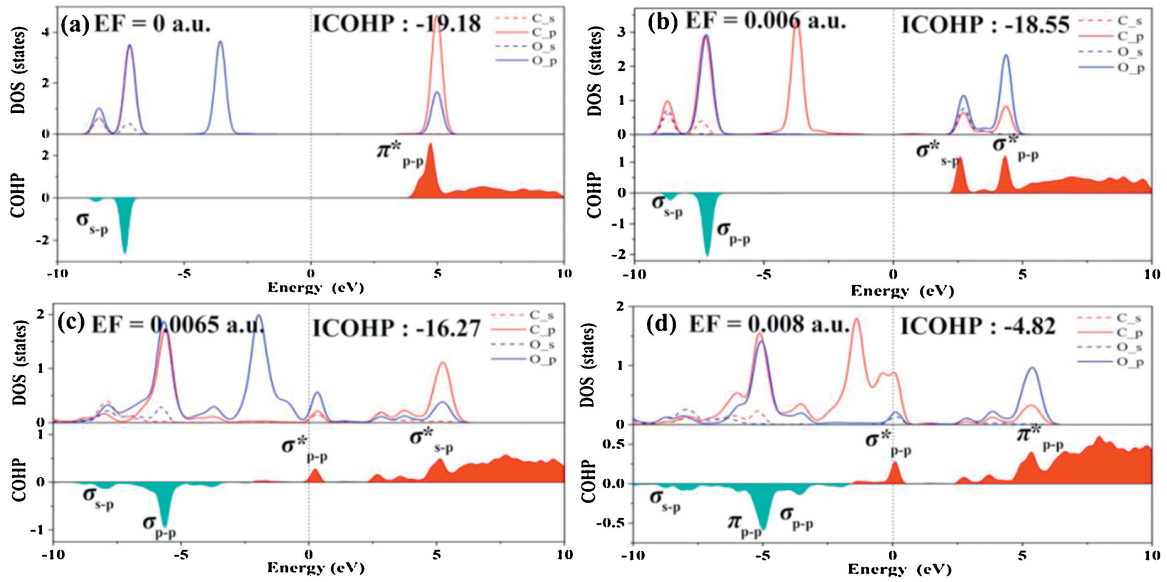

Fig. 3. PDOS (partial density of states) and molecular orbital of CO_2 molecule adsorbed on BC_3 under different E-field values, above and below the 0 value of crystal orbital hamiltonian population (COHP) are the anti-bonding state and bonding state, respectively. Red stands for bonding contributions, while cyan stands for antibonding contributions.

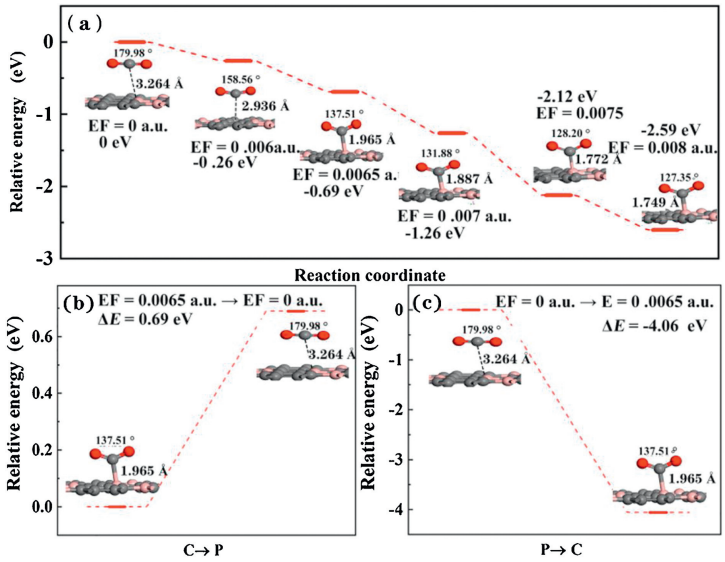

Fig. 4. The energy profile for the chemisorption to physisorption of the adsorbed CO_2 over BC_3 due to removing or switching of E-field (EF = 0.0065 a.u.).

CH_4 and H_2 are high-quality energy gases and important raw materials for the manufacture and synthesis of many chemical products. However, in the actual production and processing of CH_4 and H_2, the presence of CO_2 impurities will inevitably be introduced. Therefore, the separation of CO_2 from the $CO_2/H_2/CH_4$ mixed gas is of great research significance for improving the purity of CH_4 and H_2. In order to evaluate the separation effect of the electric field on the $CO_2/CH_4/H_2$ mixed gas, we studied the adsorption behavior of BC_3 to $CO_2/CH_4/H_2$ under the E-Field of 0.004 and 0.0065 a.u.. In the external E-Field of 0.004 a.u., the most stable adsorption structure is shown in Fig. S7 (Supporting information). The adsorption distances of $CO_2/H_2/CH_4$ on the BC_3 substrate are 3.032, 2.118, and 2.952 Å, and the corresponding E_{ads} are –0.35, –0.43 and –0.38 eV, respectively. No obvious electron distribution was observed between the CO_2/CH_4 gas molecules and the substrate. According to the difference in adsorption energy, it can be concluded that H_2 can be efficiently separated from the $CO_2/H_2/CH_4$ mixed gas under the 0.004 a.u.. In addition, the adsorption behaviors of $CO_2/H_2/CH_4$ gas under an electric field of 0.0065 a.u. has been studied, which is shown in Fig. S8 (Supporting information). Differ from the physical adsorption of $CO_2/H_2/CH_4$ under no electric field (Fig. S2.), the E_{ads} and D_m of CO_2 change significantly (-0.11 to -0.84 eV, 3.371 to 1.965 Å). There is no electron density distribution between the H_2/CH_4 and the BC_3 substrate, but there is a distinct electron density overlaps between the CO_2 and the substrate, as shown in Fig. S8. Obviously, the adsorption properties of CO_2 and H_2/CH_4 are different, under this circumstance the former is chemical adsorption and can be captured by BC_3, but in fact the latter is physical adsorption.

We used the spin-polarized DFT calculation method to study the adsorption/desorption behavior of CO_2 gas with an external Z-axis vertical positive electric field. An external electric field

vertical to the BC_3 surface can significantly enhance the interaction between CO_2 and the substrate. In particular, in the range of 0.006-0.0065 a.u. electric field value, CO_2 shifted from BC_3 physisorption on C_4B_2 vacancy with the rapid decrease of E_{ads} by 663% (–0.11 to –0.84 eV). Desorption of chemisorbed CO_2 occurred from the BC_3 surface without passing any energy barrier and released an energy of 0.69 eV when the E-Field is switched off. Utilizing the difference in the adsorption properties of $CO_2/CH_4/H_2$ on BC_3 under the E-Field value of 0.004 and 0.0065 a.u., H_2 and CO_2 gas can be separated from the $CO_2/H_2/CH_4$ gas mixture. These results confirmed that BC_3 is a potential material for capturing CO_2 under external electric field.

Declaration of competing interest

The authors declare that they have no known competing financial interests or personal relationships that could have appeared to influence the work reported in this paper.

Acknowledgments

This study was funded by the National Natural Science Foundation of China (No. 21603109), the Henan Joint Fund of the National Natural Science Foundation of China (No. U1404216), the Scientific Research Program Funded by Shaanxi Provincial Education Department (No. 20JK0676).

Appendix A. Supplementary data

Supplementary material related to this article can be found, in the online version, at doi:https://doi.org/10.1016/j.cclet.2021.03.038.

References

[1] Y. Wang, Y. Lan, Chin. Chem. Lett. 31 (2020) 736–738.
[2] Z. Ni, S. Bao, X. Gong, Chin. Chem. Lett. 31 (2020) 1674–1679.
[3] Y. Song, X. Li, C. He, Chin. Chem. Lett. 32 (2021) 1106–1110.
[4] M. Wang, Z. Zhang, Y. Gong, et al., Appl. Surf. Sci 502 (2020) 144067.
[5] R.A. Agarwal, A.K. Gupta, D. De, Cryst. Growth & Des 19 (2019) 2010–2018.
[6] M. Kang, D.W. Kangand, C.S. Hong, Dalton. Trans. 48 (2019) 2263–2270.
[7] S. Liu, W.L. Li, J.P. Zhang, New. J. Chem. 44 (2020) 95–101.
[8] M.D. Esrafili, J. Mol, Graph. Model. 90 (2019) 192–198.
[9] G.S. Rao, T. Hussain, M.S. Islam, et al., Nanotechnology 27 (2016) 015502.
[10] S. Zhou, M. Wang, J. Wang, et al., J. Mater. Chem. A 8 (2020) 9970–9980.
[11] L.P. Guo, W.C. Li, B. Qiu, et al., J. Mater. Chem. A 7 (2019) 5402–5408.
[12] X. Liu, S. Wei, S. Zhou, et al., J. CO_2 Util. 26 (2018) 588–594.
[13] C. Wang, J. Wang, X. Xiao, G. Zhong, S. Wu, Chin. Chem. Lett. 30 (2019) 1269–1272.
[14] H. Guo, W. Zhang, N. Lu, et al., J. Phys. Chem. C 119 (2015) 6912–6917.
[15] Q. Sun, G.Q. Qin, Y.Y. Ma, et al., Nanoscale 9 (2017) 19–24.
[16] H. Tanaka, Y. Kawamata, H. Simizu, et al., Solid. State. Commun. 136 (2005) 22–25.
[17] M. Zhang, H. Liu, Q. Li, et al., Phys. Rev. Lett. 114 (2015) 015502.
[18] R.K. Zahedi, A.H.N. Shirazi, P. Alimouri, N. Alajlan, T. Rabczuk, Comp. Mater. Sci. 168 (2019) 1–10.
[19] B. Mortazavi, M. Shahrokhi, M. Raeisi, et al., Carbon 149 (2019) 733–742.
[20] L. Qin, L. Wang, X. Yang, et al., J. Catal. 359 (2018) 242–250.
[21] S. Mehdi Aghaei, M.M. Monshi, I. Torres, S.M.J. Zeidi, I. Calizo, Appl. Surf. Sci. 427 (2018) 326–333.
[22] J. Beheshtian, A.A. Peyghan, M. Noei, Sensor. Actuat. B: Chem. 181 (2013) 829–834.
[23] Q.G. Jiang, Z.M. Ao, S. Li, Z. Wen, RSC Adv. 4 (2014) 20290–20296.
[24] G. Liu, J. Zhou, W. Zhao, Z. Ao, T. An, Chin. Chem. Lett. 31 (2020) 1966–1969.
[25] K. Shin, D.H. Kim, S.C. Yeo, H.M. Lee, Catal. Today 185 (2012) 94–98.
[26] W. Wu, Z. Ao, T. Wang, C. Li, S. Li, Phys. Chem. Chem. Phys 16 (2014) 16588–16594.
[27] Z.M. Ao, F.M. Peeters, Appl. Phys. Lett. 96 (2010) 253106.
[28] H. Ji, T. Wang, T. Huang, B. Lai, W. Liu, J. Clean. Prod. 278 (2021) 123924.
[29] C. Dang, F. Sun, H. Jiang, et al., Mater 12 (2019) 676.
[30] H. Ji, P. Du, D. Zhao, et al., Appl. Catal. B: Environ. 263 (2020) 118357.
[31] G. Giorgi, K. Yamashita, Chem. Lett. 44 (2015) 826–828.
[32] T. Pauporte, O. Lupan, J. Zhang, et al., ACS Appl. Mater. Interfaces 7 (2015) 11871–11880.
[33] L. Fu, R. Wang, C. Zhao, et al., Chem. Eng. J 414 (2021) 128857.
[34] J. Wang, J.R. Huo, L. Fu, C.X. Zhao, Adv. Theor. Simul. 4 (2021) 2100003.
[35] J. Yu, C. He, C. Pu, et al., Chin. Chem. Lett. (2021), doi:http://dx.doi.org/10.1016/j.cclet.2021.02.046.
[36] L.M. Azofra, N. Li, D.R. MacFarlane, C. Sun, Energ. Environ. Sci. 9 (2016) 2545–2549.
[37] Q. Li, L. He, C. Sun, X. Zhang, Journal of Physical Chemistry C 121 (2017) 27563–27568.
[38] F. Zhou, L.M. Azofra, M. Ali, et al., Energ. Environ. Sci. 10 (2017) 2516–2520.
[39] C. Liu, Q. Li, C. Wu, et al., J. Am. Chem. Soc. 141 (2019) 2884–2888.
[40] C. Liu, Q. Li, J. Zhang, et al., J. Mater. Chem. A. 7 (2019) 4771–4776.
[41] W. Wang, H. Zhang, S. Zhang, et al., Angew. Chem. Int. Ed. 58 (2019) 16644–16650.
[42] Z. Jin, C. Liu, Z. Liu, et al., Adv. Energy. Mater. 10 (2020) 2000797.
[43] Y. Lei, Y. Wang, Y. Liu, et al., Angew. Chem. Int. Ed. 59 (2020) 20794–20812.
[44] Y. Wang, Y. Liu, W. Liu, et al., Energ. Environ. Sci. 13 (2020) 4609–4624.
[45] W. Song, J. Wang, L. Fu, et al., Chin. Chem. Lett. (2020), doi:http://dx.doi.org/10.1016/j.cclet.2021.02.043.
[46] B. Delley, J. Chem. Phys. 113 (2000) 7756–7764.
[47] J.P. Perdew, K. Burke, M. Ernzerhof, Phys. Rev. Lett. 77 (1996) 3865–3868.
[48] B. Delley, J. Chem. Phys. 92 (1990) 508–517.
[49] S. Grimme, J. Antony, S. Ehrlich, H. Krieg, J. Chem. Phys. 132 (2010)154104.
[50] G. Song, Z. Yi, L. Xie, et al., Chin. Chem. Lett. 31 (2020) 1392–1397.
[51] K. Belasfar, M. Houmad, M. Boujnah, A. Benyoussef, A.E. Kenz, J. Phys. Chem. Solid. 139 (2020)109319.
[52] Q. Yue, Z. Shao, S. Chang, J. Li, Nanoscale. Res. Lett. 8 (2013) 425.
[53] J. Zhao, J.W. Jiang, Y. Jia, W. Guo, T. Rabczuk, Carbon 57 (2013) 108–119.
[54] L. Chen, C. He, R. Wang, et al., Chin. Chem. Lett. 32 (2021) 53-56.
[55] G.Q. Qin, A.J. Du, Q. Sun, Energy Technol. 6 (2018) 205–212.
[56] C. He, R. Wang, H. Yang, S. Li, L. Fu, Appl. Surf. Sci. 507 (2020) 145076.
[57] C. He, R. Wang, D. Xiang, et al., Appl. Surf. Sci. 509 (2020) 145392.
[58] X. Li, T. Guo, L. Zhu, et al., Chem. Eng. J. 338 (2018) 92–98.
[59] A.A. Khan, I. Ahmad, R. Ahmad, Chem. Phys. Lett. 742 (2020) 137155.
[60] M.D. Esrafili, J. Mol, Graph. Model. 90 (2019) 192–198.
[61] L. Li, L. Shi, X. Yu, et al., Chin. Chem. Lett. 30 (2019) 1147–1152.
[62] Z.H. Chen, Z. Xie, P. Natl. A. Sci, India. A. 90 (2018) 1–10.
[63] S. Steinberg, R. Dronskowski, Crystals 8 (2018) 225.
[64] V.L. Deringer, A.L. Tchougreeff, R. Dronskowski, J. Phys. Chem. A 115 (2011) 5461–5466.
[65] J. Jin, J. Chen, H. Wang, P. Hu, Chin. Chem. Lett. 30 (2019) 618–623.